

All-Electron APW+*lo* calculation of magnetic molecules with the SIRIUS domain-specific package

Long Zhang,^{1,2,3} Anton Kozhevnikov,⁴ Thomas Schulthess,⁴ S. B. Trickey,^{1,2,3} and Hai-Ping Cheng^{1,2,3, a)}

¹⁾*Department of Physics, University of Florida, Gainesville, FL 32611, USA*

²⁾*Quantum Theory Project, University of Florida, Gainesville, FL 32611, USA*

³⁾*Center for Molecular Magnetic Quantum Materials, University of Florida, Gainesville, FL 32611, USA*

⁴⁾*Swiss National Supercomputing Centre, Zurich, Switzerland*

(Dated: Dec. 2, 2022)

We report APW+*lo* (augmented plane wave plus local orbital) density functional theory (DFT) calculations of large molecular systems using the domain specific SIRIUS multi-functional DFT package. The APW and FLAPW (full potential linearized APW) task and data parallelism options and advanced eigen-system solver provided by SIRIUS can be exploited for performance gains in ground state Kohn-Sham calculations on large systems. This approach is distinct from our prior use of SIRIUS as a library backend to another APW+*lo* or FLAPW code. We benchmark the code and demonstrate performance on several magnetic molecule and metal organic framework systems. We show that the SIRIUS package in itself is capable of handling systems as large as a several hundred atoms in the unit cell without having to make technical choices that result in loss of accuracy with respect to that needed for study of magnetic systems.

^{a)}Electronic mail: hping@ufl.edu

I. INTRODUCTION

Molecular magnetism, notably in the context of molecular magnetic materials, is a very active interdisciplinary research area that has significant implications for computational investigations. Motivated in no small measure by the promise of high impact on quantum computing^{1,2}, molecular magnetism deals with design, synthesis, and physical and chemical characterization of single-molecule magnets (SMMs)^{3,4}, spin-crossover molecules⁵⁻⁸ and condensed aggregates thereof. Predictive and interpretive first-principles calculations are valuable both for experimental progress and for formulation and parametrization of models of the molecular spin systems. We begin therefore with a brief overview of the physical problem class, then turn to attendant computational challenges and some progress in meeting them.

A. Motivation from physical systems

Molecular magnetism involves a large range of dimensionality, from isolated SMMs^{9,10} and 1D chain magnets^{11,12} through 2D molecular layers¹³ to 3D polymers and metal organic framework^{14,15} materials that exhibit collective ordering of magnetic moments.

Growing research activity, both theoretical and experimental, has focused on (1) low dimensional materials (motivated by their potential application in high-density magnetic storage and nano-scale devices)^{16,17} and (2) so-called functional materials^{9,16,18,19} (because of their strong response to changing external conditions). Because molecular magnets have well-localized magnetic moments, they provide a nearly perfect arena for investigation of intriguing phenomena and testing models. Distinct from bulk magnetic materials, their quantum size effects suggest applications beyond conventional high-density information storage. Example applications include spintronics and qubits for quantum computing.

The molecules involved are large and rather complicated. An example category is Mn₁₂ complexes²⁰. Their investigation dates to synthesis by Weinland and Fischer in 1921²¹, yet the crystal structure was not determined until 1980²². That particular Mn₁₂ molecule is built from four Mn₄₊ ($S = 3/2$) and eight Mn₃₊ ($S = 2$) ions coupled by oxygen atoms. The [Mn₁₂O₁₂(O₂CPh)₁₆(H₂O)₄] complex was studied beginning in 1988,²³ and its ground state eventually determined^{24,25} to have $S = 10$. For computational context, note that this

system has 176 atoms and 1210 electrons.

A major class of experimental effort has focused on design and synthesis of multi-nuclear clusters containing⁴ Mn^{3+} , because the axially Jahn-Teller distorted Mn^{3+} ionic positions usually cause large magnetic anisotropy due to spin-orbital coupling. A large number of Mn(III)-based SMMs has been reported, including those with Mn_6 ²⁶, Mn_{19} ^{27–29}, Mn_{25} ^{30,31}, Mn_{31} ³² and Mn_{84} ³³. In addition, many transition metal (TM) SMMs based upon anisotropic V^{3+} , $\text{Fe}^{2+/3+}$, Ni^{2+} , and Co^{2+} ions have been synthesized; see Refs. 3, 34–39. The octa-nuclear cluster $[\text{Fe}_8\text{O}_2(\text{OH})_{12}](\text{tacn})_6]^{8+}$ (Fe^8), where (tacn) is the organic compound $\text{C}_6\text{H}_{12}(\text{NH})_3$, reported by Sangregorio et al.³⁵ is an example. It has 174 atoms and 756 electrons with a $S = 10$ ground state that arises from competing anti-ferromagnetic interactions among eight Fe^{3+} ($S = 5/2$) ions⁴⁰. Magnetic measurements revealed that it has an anisotropy energy barrier of 17cm^{-1} induced by magnetic anisotropy. This is much smaller than that of the Mn_{12} complexes. Other significant synthesis effort has been focused on enhancing the magnetic anisotropy of the molecule^{41–44}. That has stimulated the development of several different groups of SMMs, including cyano-bridged SMMs^{45–47}, Ln-based SMMs^{48–52}, $3d$ - $4f$ -element-based SMMs^{50,53}, actinide-based SMMs⁵¹, radical-bridged SMMs⁵⁴ and organo-metallic SMMs⁵⁵.

The critical setting regarding insightful computational studies provided by this brief overview is straightforward. SMMs are large, structurally and electronically intricate molecules with complicated spin manifolds. Materials comprised of them are, of necessity, more complicated and demanding. Many of the chemical details of SMMs are largely irrelevant to that assessment. However, the presence of heavy nuclei and the importance of anisotropy both suggest the significance of relativistic effects, including spin-orbit coupling. Predictive, materials-specific simulations of systems composed from SMMs thus are extremely challenging. Spin crossover systems pose quite similar challenges.

B. Predictive computational approaches

At present, density functional theory (DFT)⁵⁶ is the most widely used first-principles calculation method in material science. It is based on the Hohenberg-Kohn theorems that show that the ground-state observables of an interacting many-electron system are functionals of the ground-state charge density, and that the total energy functional is variational with

respect to the density⁵⁶. As is well known, the HK theorems do not provide a procedure for constructing the variational functional. That was provided by Kohn and Sham who introduced an auxiliary system of non-interacting fermions that also obey the HK theorems⁵⁷. The non-interacting system has a one-body Schrödinger equation that delivers the ground state charge density, hence enables evaluation of the variational energy.

With an appropriate basis set, one can expand the Kohn-Sham (KS) orbitals, potential v_{KS} , and charge density and convert the KS equations to a set of linear equations that can be solved using refined, efficient eigen-system methods. Since v_{KS} is a density functional, the KS equations must be solved by self-consistent iterative methods⁵⁸.

The all-electron full-potential linearized augmented plane wave (FLAPW) basis is one well-tested form for implementation of the KS problem. A related form is APW+*lo*, augmented plane waves plus local orbitals. This family of basis sets is based on a partitioning of the unit cell of a material into non-overlapping muffin-tin (MT) spheres, centered at the atomic nuclei, and an interstitial (IS) region between the MT spheres, as illustrated in Fig. 1.

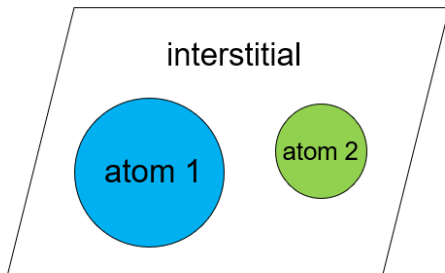


FIG. 1. Muffin-tin partitioning of a unit cell.

These basis sets originated from the APW method proposed by Slater^{59,60}. It involved a non-linear eigenvalue problem for the determination of the MT basis functions themselves. A significant step forward was the introduction of linearized methods by Andersen⁶¹ and applied by Koelling and Arbman⁶² using the muffin-tin approximation to the potential. They also pointed out that the FLAPW made non-muffin-tin calculations feasible. The basis set is constructed according to the same space partition. One piece of the basis function for Bloch

wave-vector \mathbf{k} and plane-wave vector \mathbf{G} is

$$\varphi_{\mathbf{k}}^{\mathbf{G}}(\mathbf{r}) = \begin{cases} \sum_{\ell, m} \sum_{\nu} A_{\ell m \nu}^{\alpha, \mathbf{k}}(\mathbf{G}) u_{\ell \nu}^{\alpha}(r) Y_{\ell m}(\hat{\mathbf{r}}), & \mathbf{r} \in \alpha \\ (1/\sqrt{\Omega}) e^{i(\mathbf{G}+\mathbf{k})\cdot\mathbf{r}}, & \mathbf{r} \notin \alpha \end{cases} \quad (1)$$

Here $u_{\ell \nu}^{\alpha}(r)$ is the solution of the (energy dependent) radial Schrodinger equation in the MT sphere labeled α , $Y_{\ell m}(\hat{\mathbf{r}})$ are spherical harmonics, $A_{\ell m \nu}^{\alpha, \mathbf{k}}(\mathbf{G})$ are the matching coefficients for connection with the interstitial plane wave, ℓ and m are the azimuthal and magnetic quantum numbers in a particular sphere, and ν is the order of energy derivative of the radial function. The APW basis set does not have continuous radial first derivatives at the sphere boundaries. The dependence of the radial functions upon the energy for which they are solved is the APW basis difficulty. Continuity at sphere boundaries requires those energies to correspond to KS eigenvalues. That correspondence makes the KS secular equation highly non-linear in the one-electron energies. The problem is remedied by introducing the energy derivative of the radial function to the basis, $\dot{u}_{\ell \nu}^{\alpha} = [\partial/\partial\epsilon]u_{\ell \nu}^{\alpha}$. The resulting linearized APW (LAPW) basis is ordinary, in the sense of being decoupled from explicit dependence on the KS eigenvalues. The basis can be enhanced by addition of local orbitals (*lo*), which are radial functions and energy derivatives that vanish at the MT boundaries.

For any of these APW-based forms, the electron density and the effective potential are expanded in correspondence to the space division in the unit cell. In the interstitial region they are expanded in plane waves, while inside the MT spheres the expansion is in real spherical harmonics $R_{\ell m}(\mathbf{r})$:

$$n(\mathbf{r}) = \begin{cases} \sum_{\ell m} n_{\ell m}^{\alpha}(r) R_{\ell m}(\hat{\mathbf{r}}), & \mathbf{r} \in \alpha \\ \sum_{\mathbf{G}} \tilde{n}(\mathbf{G}) e^{i\mathbf{G}\cdot\mathbf{r}}, & \mathbf{r} \notin \alpha \end{cases} \quad (2)$$

and

$$v_{KS}(\mathbf{r}) = \begin{cases} \sum_{\ell m} v_{\ell m}^{\alpha}(r) R_{\ell m}(\hat{\mathbf{r}}), & \mathbf{r} \in \alpha \\ \sum_{\mathbf{G}} \tilde{v}(\mathbf{G}) e^{i\mathbf{G}\cdot\mathbf{r}}, & \mathbf{r} \notin \alpha. \end{cases} \quad (3)$$

Here $n_{\ell m}^{\alpha}(r)$, $\tilde{n}(\mathbf{G})$, $v_{\ell m}^{\alpha}(r)$, and $\tilde{v}(\mathbf{G})$ are expansion coefficients determined through the self-consistent solution of the KS equation.

Notice that the muffin-tin decomposition of the unit cell is used solely for constructing the basis functions and expanding various quantities. The KS equation that is solved has no shape approximation, hence the phrase “full-potential”. There also is no reliance on pseudo-potentials or projector augmented waves. Thus FLAPW and APW+*lo* solutions are all-electron treatments. For that reason, they commonly are considered and used as a highly precise (“gold standard”) realization of DFT against which the precision of other computational implementations of DFT is tested.

Precisely because the methods using APW-type basis sets are full potential and all-electron, there is a serious issue for using them as gold-standard tests in large-scale computational investigations of molecular magnetic materials. That key issue is efficient use of machine resources and achievement of meaningful computational speed. Addressing that issue motivates the focus of the present work upon the domain-specific SIRIUS package. The design goal of SIRIUS was to achieve computational efficiency. Our goal here is to exploit SIRIUS to make fast and efficient all-electron, full-potential DFT calculations routinely feasible for large and complicated systems as exemplified by magnetic molecules and their aggregates. In the following sections, first we describe the package and its intended usage for accelerating plane-wave based DFT codes. We then explain its value when used as a stand-alone FLAPW/APW+*lo* package. Then we demonstrate its capabilities by calculations on a selection of magnetic molecules.

II. THE SIRIUS PACKAGE

Irrespective of the particular code, FLAPW/APW+*lo* calculations obviously have the same underlying formalism. Because those basis sets start from plane waves, such codes also have significant elements in common with plane-wave pseudo-potential (PW-PP) codes. Those elements include: unit cell setup, atomic configurations, definition and generation of reciprocal lattice vectors \mathbf{G} and combinations with Bloch wave vectors $\mathbf{G} + \mathbf{k}$, definition of basis functions on regular grids as Fourier expansion coefficients; construction of the plane-wave contributions to the KS Hamiltonian matrix, generation of the charge density, effective potential, and magnetization on a regular grid; symmetrization operations on the charge density, potential and occupation matrix; iteration-to-iteration mixing schemes for density and potential; diagonalization of the secular equation. As already is evident, compared to PW-

PP codes, FLAPW/APW+*lo* codes also have everything expanded in radial functions and spherical harmonics inside the MT spheres, along with enforcement of matching conditions on sphere surfaces.

As we have discussed elsewhere⁶³, those commonalities offer an opportunity, namely *separation of concerns*. For those generally common tasks in FLAPW/APW+*lo* and PW-PP codes, the concept is to create a performance-optimized package with enough user support that it can be exploited either as a basic code or as a library. This strategy allows the abstraction and encapsulation of the common objects just listed, thereby exposing opportunities for optimizing computational performance irrespective of the user interface (input, post-processing, etc.). The SIRIUS package was designed from the outset and developed from the outset with that goal. It provides both task and data parallelization. It is optimized for multiple MPI levels as well as OpenMP parallelization and for GPU utilization as well.

SIRIUS can be interfaced directly with both existing FLAPW/APW+*lo* codes and with PW-PP codes as a *DFT library*. We have presented an example of such use elsewhere⁶³. Though that was the originally intention for the primary usage of SIRIUS, it turns out to have some limitations imposed by design incompatibilities structured into the host code. However, SIRIUS does have basic FLAPW/LAPW+*lo* stand-alone capability. Thus there is opportunity to see what benefits can be gained for large-scale magnetic system calculations in that mode of SIRIUS usage.

A few details about SIRIUS are relevant. It is written in C++ along with the CUDA⁶⁴ backend to provide several features: (1) low-level support such as pointer arithmetic and type casting as well as high-level abstractions such as classes and template meta-programming; (2) easy interoperability between C++ and widely used Fortran90; (3) full support from the standard template library (STL)⁶⁵; (4) easy integration with the CUDA `nvcc` compiler⁶⁶. Though not relevant here, SIRIUS provides dedicated API functions for interfacing to the QuantumEspresso and *exciting* codes.

Motivated by the demands of large-system calculations, SIRIUS is designed and implemented with both task distribution and data (large array) distribution in mind. Note that typical KS calculations in a basis set rely on two basic functionalities, distributed complex matrix-matrix multiplication (`pzgemm` in LAPACK⁶⁷) and a distributed generalized eigenvalue solver (`pzhgvx` also in LAPACK). SIRIUS handles these two major tasks with data

distribution and multiple levels of task distribution.

For computational capability, switching from LAPACK to ScaLAPACK gives the benefit of data parallelism but does not remove the diagonalization algorithm limitation. Switching from LAPACK (or ScaLAPACK) to a Davidson-type diagonalization addresses that. Doing so requires taking into consideration both the diagonalization algorithm and the handling of large data sets as the system size grows. This is especially so in the case of iterative diagonalization implemented in FLAPW/LAPW+*lo* basis codes. When the unit cell is as large as ten Å³ and contains a hundred or more multi-electron atoms, the plane-wave cutoff needed is normally about 25–30 a_0^{-1} (where a_0 is the Bohr radius) to reach a properly converged ground state. This causes the reciprocal-lattice-vector (G -vector) related arrays to become very large.

The problem is illustrated by the ELK and *exciting* codes. Each has several multi-dimensional arrays that have one dimension for the global G -vector indices. Because those arrays are not handled in a distributed way, they become very memory consuming in a single MPI task. Eventually they become the real bottleneck, once the diagonalization algorithm limitation is removed via a Davidson-type method. SIRIUS, in contrast, treats the G -vector related multi-dimensional arrays in distributed manner by design.

As noted already, standard libraries do not offer Davidson-type diagonalization algorithms because they utilize repeated application of the Hamiltonian to a sub-space of the system. Algorithmic implementation therefore depends on construction details of the Hamiltonian matrix, i.e. it depends on the specific DFT formalism. Again, the SIRUS package takes this into consideration by design. It provides an efficient implementation of Davidson-type diagonalization⁶⁸ for both FLAPW/APW+*lo* and PW-PP codes.

With the foregoing discussion for context, we turn to examples of stand-alone SIRIUS calculations on large molecular magnetic and spin crossover systems that exemplify our interests.

III. SIRIUS: [MN(TAA)] MOLECULE

Because it has proven to be a difficult case⁸, the first system studied is a molecular spin crossover (SCO) complex called [Mn(taa)]. Such systems often are found in transition metal compounds and metal organic frameworks. The SCO transition can be induced by a variety

of external perturbations, e.g. as temperature, pressure, magnetic, and electric field. SCO molecular materials have potential utility for reversible molecular switching in functional materials. The [Mn(taa)] molecule ($[Mn^{3+}(pyrol)_3(tren)]$) is a meridional pseudo-octahedral chelate complex of a single Mn ion as the magnetic center and the hexadentate tris[(E)-1-(2-azolyl)-2-azabut-1-en-4-yl]amine ligand. It has 53 atoms and 224 electrons. Originally studied by Sim and Sinn⁶⁹, it was the first known example of a Mn(III) $3d^4$ SCO system. Experimentally it is an example of a transition that can be induced by application of an external magnetic field. Without any external magnetic field, the Mn^{3+} cation goes from a low-spin (LS) state (S=1) to a high-spin (HS) state of (S=2) at a transition temperature of about 45 K. The total energy difference between LS and HS states, $\Delta E_{HL} = E_{HS}^{tot} - E_{LS}^{tot}$, is relatively small, which makes magnetic-field-induced SCO transition experimentally feasible. Since the SCO is caused by the change of $3d$ electron configuration, the transition to the HS state is accompanied with not only a variation of dielectric constant but also an enhancement of the lattice volume. An important feature of the SCO transition of [Mn(taa)] is that the reorientation of the electric dipole moments appears to arise from the dynamic Jahn-Teller (JT) effect in the HS state⁷⁰. Detailed first-principles calculation in combination with Monte Carlo simulation disclosed three competing HS phases: a Jahn-Teller ordered (solid) phase, a dynamically correlated (liquid) phase, and an uncorrelated (gas) phase⁷¹. The system poses challenges to the computational determination of the ground state due to the aforementioned small scale of ΔE_{HL} relative to the total energy magnitudes. Estimates are about 50 ± 30 meV but as high as a few hundred meV depending upon the exchange-correlation (XC) approximation used and various technical details⁸. Note that usual XC approximations suffer from a self-interaction error and hence tend to favor the LS state to reduce spurious self-repulsion with the result of overestimated ΔE_{HL} values. That is not a concern in the current work since what we are testing is the capability of SIRIUS in finding the LS ground state.

Several factors can affect a DFT calculation of the molecular ground state significantly. For consistency with condensed phase calculations, it is appropriate to study the isolated molecule in a large, periodically bounded box. To attain required accuracy, the plane wave cutoff needs to be large. For the isolated molecule, the vacuum volume in the computational unit cell requires even larger cutoffs. This makes the APW+*lo* calculation an intensive job because of the comparatively large Hamiltonian matrix to be diagonalized and the large

G -vector related arrays.

The quality of APW+*lo* calculations is governed by the dimensionless quantity $R_{min}^{MT} \cdot |\mathbf{G}^k|_{max}$, where R_{min}^{MT} is the minimum muffin-tin radius of all atomic species and $|\mathbf{G}^k|_{max}$ is the maximum $\mathbf{G} + \mathbf{k}$ vector magnitude. A common default value of $R_{min}^{MT} \cdot |\mathbf{G}^k|_{max}$ is 7 in most FLAPW/APW+*lo* codes. It can be 10 if one wants to push the accuracy of total energy to be close to μ Ha. For organic molecules, the smallest R^{MT} is normally around $1.4 a_0$ for an H atom, which puts $|\mathbf{G}^k|_{max} \in [5, 7] a_0^{-1}$. The size of the Hamiltonian matrix in the first variational step is determined by $|\mathbf{G}^k|_{max}$, the total number of atoms and the local orbitals added to each atom.

For [Mn(taa)], if one sets $R_{min}^{MT} \cdot |\mathbf{G}^k|_{max} = 7$ and other parameters as shown in Table II, the dimension of the first variational Hamiltonian matrix is about 330,000. This is actually within the theoretical limit of the full diagonalization algorithm in LAPACK. However, in order to run the DFT calculation, not only the \mathbf{G}^k vectors but also the \mathbf{G} vectors for expanding density and potential must be handled efficiently. For molecules in a large cubic unit cell of the size of 20 Å with irregular vacuum space, we found (from SIRIUS calculations) that the $|\mathbf{G}|$ for density and potential needs to be as large as 25–30 a_0^{-1} to make the total energy converge. If the arrays containing \mathbf{G} vector indices are not stored in a distributed way, they become the major memory consuming quantities, which makes the calculation very slow.

The difficulty is real. We have tried to use community codes such as ELK and Exciting-Plus to calculate the ground state of [Mn(taa)] and found it to be quite difficult. If one performs a single k -point calculation for an isolated system, the lack of band parallelism within a k -point makes the run have only one MPI task. As just noted, the large $|\mathbf{G}|$ cutoff needed for density and potential implicates significant memory allocation that makes the calculation slow. A test to run the [Mn(taa)] system using Exciting-Plus on the NERSC Cori system (128GB memory per node) with $|\mathbf{G}| = 30 a_0^{-1}$ or larger caused a crash out-of-memory (OOM) error, even if one node was assigned with only one MPI task.

To have a more specific measure of the memory issue we ran the same test on the Univ. Florida HiperGator HPC large memory node and observed the peak memory consumption values reported in Table-I.

For the SIRIUS calculation of [Mn(taa)], we used the experimentally determined low spin structures and the PBE⁷² generalized gradient approximation (GGA) XC functional. We

$ \mathbf{G} _{max} (a_0^{-1})$	20	25	30	35
peak memory (GB)	39.5	110.8	151.8	209.5

TABLE I. Peak memory consumption of single k -point [Mn(taa)] calculation in a cubic unit cell of 20 Å. Other input parameters were the same as Table.II.

set $R_{min}^{MT} \cdot |\mathbf{G}^k|_{max} = 5$, $|\mathbf{G}|_{max} = 30 a_0^{-1}$, and other input parameter values listed in Table-II. There was no Hubbard U . The same structures and XC were used in a VASP⁷³ calculation for comparing the results; see Table-II.

The ground state HOMO-LUMO gap from SIRIUS is 3% larger than that from the VASP calculation. The difference is small so that it does not suggest significant difference in physical or chemical properties. The total magnetization for the two calculations agrees at 2.00 μ_B . The Mn atom moments are 1.68 μ_B and 1.77 μ_B from SIRIUS and VASP respectively. The difference arises from the fact that the muffin-tin radius for Mn in SIRIUS is 2.2 a_0 , compared to the smaller PAW projector radius of for Mn in VASP, which is 2.8 a_0 . We defer comparative discussion of average time per SCF iteration to Section V.

The benefit of this particular study is to show that SIRIUS can be used in “gold-standard” mode in studies of large molecular complexes, hence to confirm, in particular, that our previous VASP calculations on the [Mn(taa)] complex were sufficiently accurate for the purpose.

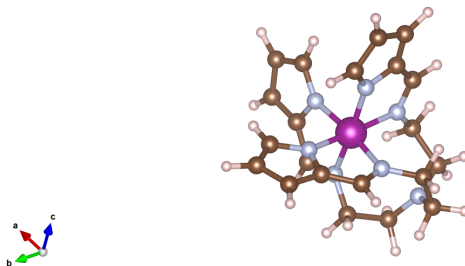


FIG. 2. [Mn(taa)] molecule

TABLE II. Input parameters for the [Mn(taa)] LS state

structure	Mn-taa, LS state structure
unit cell	$20 \times 20 \times 20 \text{ \AA}$ box
number of atoms	53
$R_{mt} (a_0)$	Mn: 2.2; O: 1.6; C: 1.4; H: 1.0;
$R_{min}^{MT} \cdot \mathbf{G}^k _{max}$	5
$ \mathbf{G}_{max} (a_0^{-1})$ for ρ and V_{eff}	30
l_{max} for APW	8
l_{max} for ρ and V_{eff}	8
size of 1st variational Hamiltonian	$\approx 155,000$
k -point grid	$1 \times 1 \times 1$
(L)APW configuration	$\epsilon_l = -0.15 \text{ eV}$; $\partial_E = 0$;
lo configuration	Mn: s, p, d ; O/C: s, p ; H: s ;
treated as core state	Mn: 1s, 2s, 2p, 3s; O/C: 1s
total energy tolerance	10^{-6} Har
potential tolerance	10^{-7} Har
run job setup:	16 MPI tasks 16 OMP threads per task
number of SCF iterations	75
average time per SCF iteration	55 s
HOMO-LUMO gap (eV)	0.68 (VASP: 0.66)
$\mu_{tot} (\mu_B)$	total: 2.00 (VASP: 2.00) Mn atom: 1.68 (VASP: 1.77)

IV. SIRIUS: Mn_3 DIMER MOLECULE

One highly desirable property to demonstrate for potential application of SMMs would be quantum mechanical coupling of two or more SMMs either to one other or to a surface or other device component, all the while retaining their isolated-molecule magnetic properties to a useful degree. For this, an SMM-SMM coupled structure was identified for hydrogen-bonded supramolecular pairs of $S = 9/2$ SMMs $[\text{Mn}_4\text{O}_3\text{Cl}_4(\text{O}_2\text{CEt})_3(\text{py})_3]^{74-76}$.

Since hydrogen-bonded inter-SMM interactions do not provide easy control of oligomerization nor guarantee retention of the oligomeric structure in solution, covalently organic linked SMM-SMM structures were developed.

The first along that line was the $[\text{Mn}_3]_4$ SMM tetramer⁷⁷, which is covalently linked with dioximate linker groups. A recent further development is the $[\text{Mn}_3]_2$ dimer molecule⁷⁸, comprised of two Mn_3 units covalently joined via dpd2-dioximate linkers. The two triangular Mn_3 units are parallel and the inter- Mn_3 interaction has been determined to be ferromagnetic. There is no experimental evidence for noticeable interactions between the two Mn_3 units. That is consistent with the absence of significant inter- Mn_3 contacts in the structure and the relatively large distance between Mn ions. The interaction quantum mechanically couples the two Mn_3 units. The structure is robust and resists any significant deformation or distortion that might affect the weak inter- Mn_3 coupling.

With the same consideration as for $\text{Mn}[(\text{taa})]$, we studied the isolated $[\text{Mn}_3]_2$ SMM dimer in a large periodically bounded box to be consistent with condensed phase calculations and to be assured of isolation. Note that $[\text{Mn}_3]_2$ has 137 atoms and 748 electrons, which is a much larger system than $\text{Mn}[(\text{taa})]$.

There is an important distinction. Both the $[\text{Mn}_3]_2$ SMM dimer and $[\text{Mn}(\text{taa})]$ calculations are done with a single k -point. Both relied upon the band parallelization in SIRIUS. The next two (see below) rely on that band parallelization as well. Both of those are metal-organic framework structures that do not have irregular vacuum regions and can use moderate Brillouin zone scan meshes, hence k -point parallelization as well. As with the $[\text{Mn}(\text{taa})]$ example, this $[\text{Mn}_3]_2$ SMM dimer calculation also benefits from distributed storage of the G -vector related arrays.

Specifically, the molecule also was placed in a 20 Å periodically bounded box with single k -point Brillouin Zone sampling. The G_{max} cutoff and LO/*lo* configuration for the Mn atoms were the same as for $[\text{Mn}(\text{taa})]$. We also used the experimental geometry⁷⁸ and the PBE XC functional⁷² (again, no Hubbard U). We are able to converge the system to the anti-ferromagnetic ground state in which there are two spin-up Mn and one spin-down Mn in each $[\text{Mn}_3]$ unit, and the total moment is zero.

The SIRIUS calculation yields similar values to those from VASP in the HOMO-LUMO gaps, which are almost identical. For the magnetization, the VASP value for the Mn ion is larger than what SIRIUS gives. Apparently this is traceable to the muffin-tin radius

(SIRIUS) being smaller than the projector cutoff radius (VASP). The average time consumed per SIRIUS SCF iteration is about 2.5 times larger than that for [Mn(taa)], but this is based on the same 16 MPI tasks for band parallelization. Increasing the number of tasks or number of cores per task would definitely make the job run faster. Comparison with VASP timings is in the next section. As with the previous study, this one shows that the SIRIUS APW+*lo* calculation can be used as a “gold-standard” to test and check VASP results.

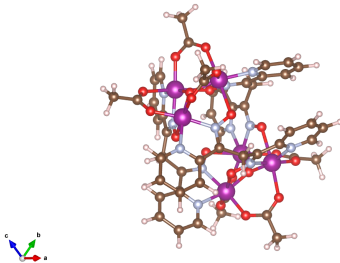


FIG. 3. Mn₃ dimer molecule

V. TIMING COMPARISON

Caution must be exercised in interpreting what follows. This is because comparison of computational costs between conceptually and structurally distinct codes is a task fraught with difficulties. Optimal resource assignments generally differ greatly not only between codes but among different machine configurations. Both the definitions and effects of precision tolerances differ between codes as well.

We compare SIRIUS only with VASP because of its very wide use and because of the cost of running the large systems studied here with other PW-PP codes. Even this restriction to one comparison involves some critical choices. Begin with MPI parallelization. We can force the two codes to run with the same number of MPI tasks, but the situations for each task are very different. The discussion that follows is specific to the NERSC Cori machine.

By experiment, we have found that the optimum number of OpenMP threads per task for SIRIUS is 16. To obtain adequate memory per task, it also is necessary to assign no more than two tasks on a node. Putting more than two on a single node degrades performance noticeably.

TABLE III. Input parameters and outputs of Mn₃ dimer

	Mn ₃ dimer
unit cell	20 × 20 × 20 Å cubic
number of atoms in unit cell	137
R_{mt} (a_0)	Mn: 2.2; O/N: 1.4; C: 1.2; H: 1.0;
$R_{min}^{MT} \cdot \mathbf{G}^k _{max}$	5
$ \mathbf{G}_{max} $ (a_0^{-1}) for ρ and V_{eff}	30
l_{max} for APW	8
l_{max} for ρ and V_{eff}	8
size of 1st variational Hamiltonian	$\approx 187,000$
k -point grid	1 × 1 × 1
(L)APW configuration	$\epsilon_l = -0.15$ eV; $\partial_E = 0$;
lo configuration ★	Mn: s, p, d ; O/C/N: s, p ; H: s
core state	Mn: 1s, 2s, 2p, 3s; O/C/N: 1s
total energy tolerance	10^{-6} Har
potential tolerance	10^{-7} Har
run job setup:	16 MPI tasks 16 OMP threads per task
number of SCF iterations	125
average time per SCF iteration	≈ 250 s
HOMO-LUMO gap (eV)	0.26 (VASP: 0.27)
μ_{tot} (μ_B)	each Mn atom (Sirius): ± 1.92 each Mn atom (VASP): ± 1.95

In contrast, for VASP the recommended practice does not require use of OpenMP. If, however, we use openMP for the sake of even-handed comparison, experiment showed that ordinarily four openMP threads per task generally is optimum (with eight at most). Thus, we can put four or more tasks per node.

Our testing was for the two systems reported above, [Mn(taa)] and Mn₃ dimer. For both we did single k -point calculations at fixed geometries with 16 MPI tasks and optimal OpenMP threads per task for each code. The choice of diagonalizer is unique in SIRIUS but

not in VASP. In it, the better choice appears to be the tag "ALGO=Fast", which invokes a mixture of the Davidson and RMM-DIIS algorithms.

With these choices, the results are that the ratio of average time per SCF iteration for VASP versus SIRIUS is about 50% for [Mn(taa)] and about 25% for the Mn₃ dimer. For [Mn(taa)] the iteration count is 75 for SIRIUS and 55 for VASP, so the rough computational cost of SIRIUS versus VASP is about a factor of 2.7. For the Mn₃ dimer, the iteration counts are 125 (SIRIUS) and 90 (VASP), so the computational cost ratio is about 5.6.

Use of the VASP "ALGO=normal" option, which invokes a blocked Davidson diagonalization algorithm, increases the VASP iteration count by about 10%, so the ratios become roughly 2.4 and 5.1 respectively.

Of course these cost ratios refer to different numbers of electrons, since SIRIUS is all-electron while VASP uses PAWs. For [Mn(taa)] the the electron count is 224 versus 156 (SIRIUS and VASP respectively) while for the Mn₃ dimer, the counts are 748 and 510 respectively. If cubic scaling with electron number (which is the most elementary expectation with Kohn-Sham calculations) is followed, the [Mn(taa)] ratio would be 2.96, not far from the observed 2.7 For Mn₃, however, cubic scaling would give 3.16. Apparently the actual 5.6 is a consequence of parallelization but we have not investigated the matter.

The larger point is that the cost-scaling, though significant, is not prohibitive even for quite large molecular systems. With that established, the next two sections give two more illustrative examples of the use of SIRIUS in the context of molecular magnetic quantum materials.

VI. SIRIUS: DTN MOLECULE

The insulating organic compound XCl₂-[SC(NH₂)₂]₄ with X=Ni or Co (DTN or DTC molecule, respectively), is a molecule-based framework structure in which magnetic and electric order can couple. It has been studied experimentally for its quantum magnetism^{79–82}. (NiCl₂-[SC(NH₂)₂]₄) has a tetragonal molecular crystal structure with two Ni atoms as magnetic centers in one unit cell. Each Ni has four S atoms and two Cl atoms as nearest neighbors, as shown in Fig. 4. They form an octahedral structure similar to the BO₆ octahedra in ABO₃ perovskites. The base octahedral structures pack in a body-centered tetragonal lattice, with Ni–Cl–Cl–Ni bonding along the *c*-axis (Fig. 4) and hydrogen bonding in the

a-b-plane. The four thiourea [SC(NH₂)₂] groups around each Ni ion are electrically polar. The *a-b*-plane components of their electric polarization cancel, while the *c*-axis components are in the same direction, thereby creating a net *c*-axis electric polarization that could be responsible for magnetic field-modified ferroelectricity.

At temperatures below 1.2 K and below a critical magnetic field, DTN is a quantum paramagnet⁸³. As the magnetic field along the *c*-axis reaches the first critical value, DTN undergoes a quantum phase transition into an XY-antiferromagnetic state in which all Ni spins lie within the *a-b*-plane. Upon further increase of the field, the spins begin to be more aligned with a corresponding increase in magnetization. When a second critical field is reached, the magnetization saturates and the material enters a spin-polarized state with all spins aligned parallel to the applied magnetic field.

There are three non-equivalent Ni-Ni spin couplings in the DTN bulk that are of interest: J_c along the *c*-axis (along the Ni-Cl-Cl-Ni bonding) between two Ni ions in adjacent unit cells, J_{ab} in the *a-b*-plane between two Ni ions in adjacent unit cells, and J_{diag} between the two Ni ions within one unit cell. Experiments suggest that the exchange coupling along the *c*-axis via the Ni-Cl-Cl-Ni chain is strong⁸⁴, and the system behaves as a quasi one-dimensional AFM chain of Ni²⁺ ions such that each ion has $S = 1$. DFT calculation can capture the main differences in values between the exchange coupling constants. A recent DFT+ U study⁸³ showed that rather large Hubbard U correction (about 5–6 eV) is needed to match experimentally fit values of the coupling constants. However the main feature, namely that J_c is about an order of magnitude larger than J_{ab} , is already captured by ordinary KS-DFT calculations without the Hubbard U correction.

Thus, we calculated J_{ab} and J_c using SIRIUS without U . To estimate the J values, we first calculate the total energy of the FM ordered and the AFM ordered states, E_{FM} and E_{AFM} , respectively. Then, assuming a Heisenberg Hamiltonian of the form $H = J[S_1 \cdot S_2]$, one can determine J from $E_{FM} - E_{AFM}$ ⁸⁵. The calculation is done using supercells, $1 \times 1 \times 2$ for J_c and $2 \times 1 \times 1$ for J_{ab} . The J_{diag} is obtained with the primitive unit cell. The supercells contain a number of atoms similar to that for the Mn₃-dimer molecule in the preceding example, namely 140 atoms and 888 electrons. The size of the supercell is approximately $10 \times 10 \times 20 \text{ \AA}^3$, about half of the cell used for both [Mn(taa)] and the Mn₃ dimer. Though the unit cell is smaller, we found proper convergence in total energy still requires a high plane-wave cutoff, $|G_{max}| = 25\text{-}30 (a_0^{-1})$, for density and potential. The input parameters are

listed in Table-IV.

Using the APW+*lo* basis and with quality parameter $R_{min}^{MT} \cdot |\mathbf{G}^k|_{max} = 6$, we can get the converged PM ground state using the primitive unit cell and the AFM and FM ground states using 1x1x2 and 2x1x1 supercells. In the AFM and FM configurations, the calculated magnetic moment of Ni is slightly smaller than the VASP value. The J_{ab} and J_c determined from the differences in total energies, Table-V, confirmed the observation obtained from using VASP. The ratio $J_{ab}/J_c \approx 8$ is actually slightly more significant than that determined by VASP, and both are in reasonable agreement with experiments. When using the primitive unit cell to determine J_{diag} , we found little differences in total energies of the FM and AFM ground state. This does not really conflict with the VASP observed 0.03 meV because the limit of the FLAPW accuracy (excluding approximations brought by XC functionals) is at 1 μ Har which is exactly 0.027 meV. The VASP-observed very small J_{diag} could be within the PAW pseudo-potential approximation error bar.

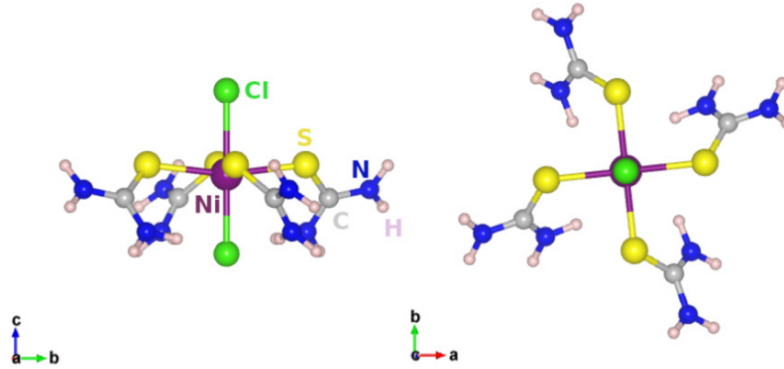


FIG. 4. base octahedral unit of DTN molecule⁸³

[H]

TABLE IV. Input parameters and outputs of DTN

	DTN $1 \times 1 \times 2$ supercell
unit cell	$\approx 10 \times 10 \times 20 \text{ \AA}$ box
number of atoms in unit cell	140
R_{mt} (a_0)	Na/Co: 2.2; Cl/S/N: 1.4; C: 1.2; H: 1.2;
$R_{min}^{MT} \cdot \mathbf{G}^k _{max}$	6
$ \mathbf{G}_{max} $ (a_0^{-1}) for ρ and V_{eff}	30
l_{max} for APW	8
l_{max} for ρ and V_{eff}	8
size of 1st variational Hamiltonian	$\approx 225,000$
k -point grid	$2 \times 2 \times 2$
(L)APW configuration for $l \leq l_{max}^{APW}$	$\epsilon_l = -0.15 \text{ eV}$; $\partial_E = 0$;
lo configuration	Na/Co: s, p, d Cl/S/C/N: s, p ; H: s
treated as core state	Ni/Co: $1s, 2s, 2p, 3s$ Cl/S/C/N: $1s$
total energy tolerance	10^{-7} Har
potential tolerance	10^{-7} Har
run job setup:	64 MPI tasks 16 OMP threads per task
number of SCF iterations	90
average time per SCF iteration	$\approx 450 \text{ s}$
HOMO-LUMO gap (eV)	0.18 (VASP: 0.18)
magnetic moment	Ni atom: ± 0.89 (VASP: ± 0.92)

	J_c (meV)	J_{ab} (meV)	J_{diag} (meV)
SIRIUS (DTN)	-2.72	-0.34	0.00
VASP (DTN) ⁸³	-1.05	-0.15	0.03

TABLE V. Exchange coupling constants from Sirius calculation compared to VASP results.⁸³

VII. SIRIUS: [Fe(*tBu*₂*qsal*)₂] MOLECULE

The [Fe(*tBu*₂*qsal*)₂] molecule is a recently created spin crossover MOF structure⁸⁶, where (*tBu*₂*qsal*) stands for 2,4-diterbutyl-6-((quinoline-8-ylimino)methyl)phenolate. The crystalized structure was determined by X-ray diffraction to be monoclinic in space group *P*2₁/*c*. It is potentially a functional molecular magnetic material because [Fe(*tBu*₂*qsal*)₂] can be sublimed at 473–573 K and 10⁻³–10⁻⁴ mbar, hence its thin-film deposition on a substrate is possible. The system undergoes a hysteretic spin transition. The average Fe–N and Fe–O bond lengths elongate from 1.949(2) Å at 100 K to 2.167(2) Å at 230 K and from 1.945(1) at 100 K to 1.997(1) Å at 230 K, respectively. These changes indicate that conversion from the LS (*S* = 0) to HS (*S* = 2) structure takes place as the temperature is increased. In addition, PW-PP-based DFT calculations⁸⁷ found the electron transfer is minimal for the molecule on a monolayer of Au(111). It suggests very small changes in the electronic structure and magnetic properties when the molecule is placed on the surface of Au.

For a system of this size, 436 atoms, 2435 electrons, we used $R_{min}^{MT} \cdot G_{max} = 4$ and other cutoffs as listed in VI. The large number of atoms does not make the Hamiltonian matrix dimension significantly larger than in the preceding cases but it makes the calculation much more time consuming. This is because the total number of radial functions of the APW functions linearly increases with the number of atoms. For each muffin-tin the radial functions are normally expanded up to $l = 8$, in comparison with the β projectors^{88,89} of the pseudo-potential method which typically are defined for *s*, *p* and *d* states only. In each SCF iteration, diagonalization of the Hamiltonian involves repeated application of the Hamiltonian to a set of wave functions. That requires summation over the APW radial functions, a task that becomes a major time consuming operation when treating large systems using APW+*lo*. For this MOF structure, we used the experimental structure and single *k*-point Brillouin zone sampling. The $R_{min}^{MT} \cdot |\mathbf{G}^k|_{max}$ was set to 4. The plane wave cutoffs for density and potential were set to 30, as before, and the angular momentum cut-off was set to the normal value, 8. Maximum benefit of band parallelization on the NERSC CORI machine (which has two 16-core CPUs and total 128GB memory per node) is reached at 8x8 MPI tasks. Each task is assigned with the resources of 16 cores thus two tasks occupy one node, which is tested to be optimal. Further increasing the number of tasks, or assigning more resources to each task, doe not seem to accelerate the calculation. With the setup

described, we managed to converge the system to non-magnetic ground state in about 80 hours. The total time needed to converge to the ground state also depends on the number of SCF iterations, which depends on the mixing algorithm for the charge density. The mixing algorithm used in the present work is the Broyden scheme⁹⁰ in which the Jacobian matrix is approximated from the previous step and improved iteratively. Other mixing schemes that implicitly approximate the inverse Jacobian from multiple previous steps, e.g. the Anderson mixing scheme⁹¹, are being tested. However adjusting and testing the mixing parameter or any other input parameter using a system of this size is not really practical, simply as a matter of resource availability. Thus the calculation of this MOF structure is a feasibility test only. We have shown meaningful KS-DFT calculations *can be done* on a system of this size using APW+*lo* and have confirmed the computational cost advantage of efficient job distribution.

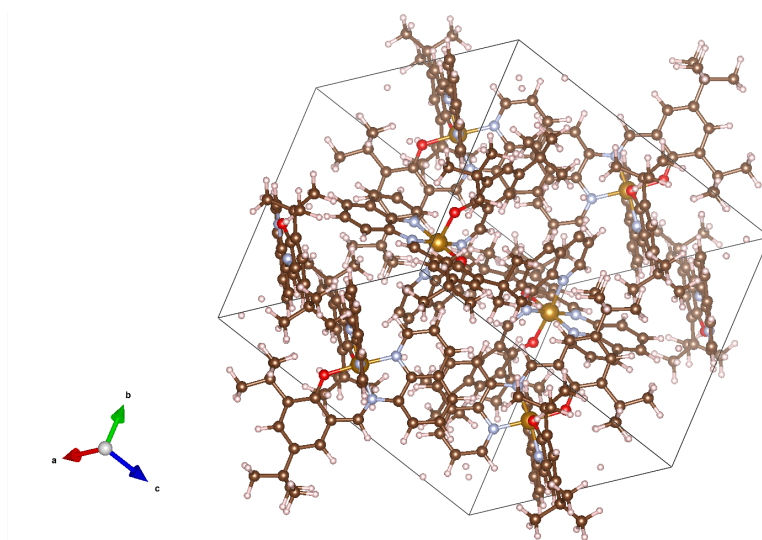


FIG. 5. the Fe4 molecule

TABLE VI. Input parameters of Fe₄ molecule, S=0

	Fe ₄ MOF
unit cell	15 × 16 × 17.5 Å
number of atoms in unit cell	436
R_{mt} (a_0)	Fe: 2.2; O: 1.4; C: 1.2; H: 1.0;
$R_{min}^{MT} \cdot \mathbf{G}^k _{\max}$	4
$ \mathbf{G}_{max} $ (a_0^{-1}) for ρ and V_{eff}	30
l_{\max} for APW	8
l_{\max} for ρ and V_{eff}	8
size of 1st variational Hamiltonian	≈ 325,000
k -point grid	1 × 1 × 1
(L)APW configuration	$\epsilon_l = -0.15$ eV; $\partial_E = 0$;
lo configuration ★	Fe: s, p, d Cl/S/C/N: s, p ; H: s
treated as core state	Ni/Co: 1s, 2s, 2p, 3s Cl/S/C/N: 1s
total energy tolerance	10 ⁻⁶ Har
potential tolerance	10 ⁻⁷ Har
run job setup:	64 MPI tasks 16 cores per task 16 OMP threads per task
number of SCF iterations	135
average time per SCF iteration	≈ 2150 s

VIII. SUMMARY AND CONCLUSION

The main purpose of this work is to demonstrate, by several concrete examples, the value of the SIRIUS architecture and implementation for all-electron KS-DFT calculations on fairly large molecules with complicated spin manifolds. By inference, this capacity extends to aggregates of such systems. SIRIUS as a stand-alone package provides performance gains through refined diagonalization methods and task and data parallelization improvements. The result is an advance in capability of the APW+*lo* DFT treatment of complex molecular aggregates.

To recapitulate, the eigenvalue solver and the distribution of G -vector arrays in community FLAPW codes, for example ELK, *exciting* and Exciting-Plus, are major bottleneck in calculations of large systems. The LAPACK/ScaLAPACK full diagonalization algorithm cannot handle Hamiltonian matrices larger than $\approx 10^6$, and the G -vector arrays cannot be handled efficiently without distributed storage. The SIRIUS package provides better data distribution and options to the use of the various (LAPACK, ScaLAPACK, Davidson) diagonalization algorithms. One can perform Davidson-type diagonalization of the Hamiltonian easily in the self-consistent loop and benefit from multiple MPI and thread-level parallelization within k -points and within bands. Together with the proper distribution of G -vector related arrays, the SIRIUS package can do plane wave based LAPW and APW+*lo* calculation of systems larger than many community LAPW/APW+*lo* codes.

We showed results from molecules using the APW+*lo* basis. The resulting total energy and magnetization are in agreement with experimental measurements and confirm corresponding VASP calculations done with PAWs. In these test calculations, good scaling in band parallelization is observed, which is particularly crucial for a single k -point calculations ([Mn(taa)], Mn₃ dimer). The results also indicate that SIRIUS parallelization works well on contemporary high performance systems and the computational time is drastically reduced compared to ELK and Exciting-Plus for example. For a system of the size of DTN supercell studied in this work, the main physical feature is captured by extraction of exchange constants J from the total energies. The results are qualitatively in agreement with experiment and VASP calculations.

Looking ahead, all-electron FLAPW and APW+*lo* calculations of medium to large molecule and MOF systems is a relatively little-explored area. It is plausible that important

core effects from, for example, spin-orbit coupling will be uncovered by such all-electron investigations. At the least, the use of plane-wave-PAW codes to drive ab initio BOMD will be validated at sample configurations by such all-electron calculations. We have shown that the SIRIUS package can handle systems as large as 200 non-H atoms routinely without losing the accuracy needed for magnetic systems. With suitable high-performance systems, SIRIUS demonstrably can be used for systems up to 430 atoms and, we surmise, larger.

Acknowledgment This work was supported as part of the Center for Molecular Magnetic Quantum Materials, an Energy Frontier Research Center funded by the U.S. Department of Energy, Office of Science, Basic Energy Sciences under Award No. DE-SC0019330. Computations were performed at NERSC and the University of Florida Research Computer Center.

REFERENCES

- ¹M. R. Wasielewski, M. D. E. Forbes, N. L. Frank, K. Kowalski, G. D. Scholes, J. Yuen-Zhou, D. E. F. Marc A. Baldo, R. H. Goldsmith, T. G. III, M. L. Kirk, J. K. McCusker, J. P. Ogilvie, D. A. Shultz, S. Stoll, and K. B. Whaley, “Exploiting chemistry and molecular systems for quantum information science,” *Nature Reviews Chemistry* **4**, 490–504 (2020).
- ²A. Gaita-Ariño, F. Luis, s. Hill, and E. Coronado, “Molecular spins for quantum computation,” *Nature Chemistry* **11**, 301–309 (2019).
- ³S. L. Castro, Z. Sun, C. M. Grant, J. C. Bollinger, D. N. Hendrickson, and G. Christou, “Single-molecule magnets: Tetranuclear vanadium(iii) complexes with a butterfly structure and an $s = 3$ ground state,” *Journal of the American Chemical Society* **120**, 2365–2375 (1998), <https://doi.org/10.1021/ja9732439>.
- ⁴R. Bagai and G. Christou, “The drosophila of single-molecule magnetism: [mn12o12(o2cr)16(h2o)4],” *Chem. Soc. Rev.* **38**, 1011–1026 (2009).
- ⁵K. P. Kepp, “Consistent descriptions of metal–ligand bonds and spin-crossover in inorganic chemistry,” *Coord. Chem. Rev.* **257**, 196–209 (2013).
- ⁶J. Cirera, M. Via Nadal, and E. Ruiz, “Benchmarking Density Functional Methods for Calculation of State Energies of First Row Spin-Crossover Molecules,” *Inorg. Chem.* **57**, 14097–14105 (2018).
- ⁷K. Kepp, “The electronic determinants in spin crossover described by density functional theory,” in *Transition Metals in Coordination Environments. Challenges and Advances in Computational Chemistry and Physics*, Vol. 29, edited by E. Broclawik, T. Borowski, and M. Radoń (Springer, 2019) pp. 1–33.
- ⁸D. Mejía-Rodríguez, A. Albavera-Mata, E. Fonseca, D.-T. Chen, H.-P. Chen, R. G. Hennig, and S. B. Trickey, “Barriers to predictive high-throughput screening for spin-crossover,” *Computational Materials Physics* **206**, 111161 (2022).
- ⁹C. Marrows, L. Chapon, and S. Langridge, “Spintronics and functional materials,” *Materials Today* **12**, 70–77 (2009).
- ¹⁰J. R. Friedman and M. P. Sarachik, “Single molecule nanomagnets,” *Annual Review of Condensed Matter Physics* **1**, 109–128 (2010), <https://doi.org/10.1146/annurev-conmatphys-070909-104053>.
- ¹¹P. L. Feng and D. N. Hendrickson, “Isostructural single-chain and single-

- molecule magnets,” *Inorganic Chemistry* **49**, 6393–6395 (2010), pMID: 20565068, <https://doi.org/10.1021/ic101016t>.
- ¹²J. L. Rong-Min Wei, Fan Cao, “Single-chain magnets based on octacyanotungstate with the highest energy barriers for cyanide compounds,” *Scientific Reports* **6** (2016), 10.1038/srep24372.
- ¹³L.-M. Zheng, J. Tang, H.-L. Sun, and M. Ren, “Low dimensional molecular magnets and spintronics,” in *Handbook of Spintronics*, edited by Y. Xu, D. D. Awschalom, and J. Nitta (Springer Netherlands, Dordrecht, 2016) pp. 617–680.
- ¹⁴A. E. Thorarinsdottir and T. D. Harris, “Metal–organic framework magnets,” *Chemical Reviews* **120**, 8716–8789 (2020), pMID: 32045215, <https://doi.org/10.1021/acs.chemrev.9b00666>.
- ¹⁵M. Kurmoo, “Magnetic metal–organic frameworks,” *Chem. Soc. Rev.* **38**, 1353–1379 (2009).
- ¹⁶W. W. Lapo Bogani, “Molecular spintronics using single-molecule magnets,” *Nature Materials* **7**, 179–186 (2008).
- ¹⁷J. Gómez-Segura, J. Veciana, and D. Ruiz-Molina, “Advances on the nanostructuring of magnetic molecules on surfaces: the case of single-molecule magnets (smm),” *Chem. Commun.* , 3699–3707 (2007).
- ¹⁸G. Mínguez Espallargas and E. Coronado, “Magnetic functionalities in mofs: from the framework to the pore,” *Chem. Soc. Rev.* **47**, 533–557 (2018).
- ¹⁹J. M. Frost, K. L. M. Harriman, and M. Murugesu, “The rise of 3-d single-ion magnets in molecular magnetism: towards materials from molecules?” *Chem. Sci.* **7**, 2470–2491 (2016).
- ²⁰K. Ziemelis, “The difficult middle ground,” *Nature Physics* **4**, S19 (2008).
- ²¹R. F. Weinland and G. Fischer, “Über manganiacetate und -benzoate,” *Zeitschrift für anorganische und allgemeine Chemie* **120**, 161–180 (1921), <https://onlinelibrary.wiley.com/doi/pdf/10.1002/zaac.19211200116>.
- ²²T. Lis, “Preparation, structure, and magnetic properties of a dodecanuclear mixed-valence manganese carboxylate,” *Acta Crystallographica Section B* **36**, 2042–2046 (1980), <https://onlinelibrary.wiley.com/doi/pdf/10.1107/S0567740880007893>.
- ²³P. D. W. Boyd, Q. Li, J. B. Vincent, K. Folting, H. R. Chang, W. E. Streib, J. C. Huffman, G. Christou, and D. N. Hendrickson, “Potential building blocks for molecular ferromagnets:

- [mn12o12(o2cph)16(h2o)4] with a $s = 14$ ground state,” *Journal of the American Chemical Society* **110**, 8537–8539 (1988), <https://doi.org/10.1021/ja00233a036>.
- ²⁴A. Caneschi, D. Gatteschi, R. Sessoli, A. L. Barra, L. C. Brunel, and M. Guillot, “Alternating current susceptibility, high field magnetization, and millimeter band epr evidence for a ground $s = 10$ state in [mn12o12(ch3coo)16(h2o)4].2ch3cooh.4h2o,” *Journal of the American Chemical Society* **113**, 5873–5874 (1991), <https://doi.org/10.1021/ja00015a057>.
- ²⁵R. Sessoli, H. L. Tsai, A. R. Schake, S. Wang, J. B. Vincent, K. Folting, D. Gatteschi, G. Christou, and D. N. Hendrickson, “High-spin molecules: [mn12o12(o2cr)16(h2o)4],” *Journal of the American Chemical Society* **115**, 1804–1816 (1993), <https://doi.org/10.1021/ja00058a027>.
- ²⁶E. Cremades, J. Cano, E. Ruiz, G. Rajaraman, C. J. Milios, and E. K. Brechin, “Theoretical methods enlighten magnetic properties of a family of mn6 single-molecule magnets,” *Inorganic Chemistry* **48**, 8012–8019 (2009), pMID: 19624160, <https://doi.org/10.1021/ic900992r>.
- ²⁷E. Ruiz, T. Cauchy, J. Cano, R. Costa, J. Tercero, and S. Alvarez, “Magnetic structure of the large-spin mn10 and mn19 complexes: A theoretical complement to an experimental milestone,” *Journal of the American Chemical Society* **130**, 7420–7426 (2008), pMID: 18489093, <https://doi.org/10.1021/ja800092s>.
- ²⁸O. Waldmann, A. M. Ako, H. U. Güdel, and A. K. Powell, “Assessment of the anisotropy in the molecule mn19 with a high-spin ground state $s = 83/2$ by 35 ghz electron paramagnetic resonance,” *Inorganic Chemistry* **47**, 3486–3488 (2008), pMID: 18393411, <https://doi.org/10.1021/ic800213w>.
- ²⁹E. E. Moushi, T. C. Stamatatos, W. Wernsdorfer, V. Nastopoulos, G. Christou, and A. J. Tasiopoulos, “A family of 3d coordination polymers composed of mn19 magnetic units,” *Angewandte Chemie International Edition* **45**, 7722–7725 (2006), <https://onlinelibrary.wiley.com/doi/pdf/10.1002/anie.200603498>.
- ³⁰M. Murugesu, S. Takahashi, A. Wilson, K. A. Abboud, W. Wernsdorfer, S. Hill, and G. Christou, “Large mn25 single-molecule magnet with spin $s = 51/2$: Magnetic and high-frequency electron paramagnetic resonance spectroscopic characterization of a giant spin state,” *Inorganic Chemistry* **47**, 9459–9470 (2008), pMID: 18788733, <https://doi.org/10.1021/ic801142p>.
- ³¹M. Murugesu, M. Habrych, W. Wernsdorfer, K. A. Abboud, and G. Christou, “Single-

- molecule magnets: A Mn₂₅ complex with a record $s = 51/2$ spin for a molecular species,” *Journal of the American Chemical Society* **126**, 4766–4767 (2004), pMID: 15080666, <https://doi.org/10.1021/ja0316824>.
- ³²P. Abbasi, K. Quinn, D. I. Alexandropoulos, M. Damjanović, W. Wernsdorfer, A. Escuer, J. Mayans, M. Pilkington, and T. C. Stamatatos, “Transition metal single-molecule magnets: A Mn₃₁ nanosized cluster with a large energy barrier of 60 k and magnetic hysteresis at 5 k,” *Journal of the American Chemical Society* **139**, 15644–15647 (2017), pMID: 29052991, <https://doi.org/10.1021/jacs.7b10130>.
- ³³A. J. Tasiopoulos, A. Vinslava, W. Wernsdorfer, K. A. Abboud, and G. Christou, “Giant single-molecule magnets: A Mn₈₄ torus and its supramolecular nanotubes,” *Angewandte Chemie International Edition* **43**, 2117–2121 (2004), <https://onlinelibrary.wiley.com/doi/pdf/10.1002/anie.200353352>.
- ³⁴R. Hernández Sánchez and T. A. Betley, “Meta-atom behavior in clusters revealing large spin ground states,” *Journal of the American Chemical Society* **137**, 13949–13956 (2015), pMID: 26440452, <https://doi.org/10.1021/jacs.5b08962>.
- ³⁵C. Sangregorio, T. Ohm, C. Paulsen, R. Sessoli, and D. Gatteschi, “Quantum tunneling of the magnetization in an iron cluster nanomagnet,” *Phys. Rev. Lett.* **78**, 4645–4648 (1997).
- ³⁶A. K. Powell, S. L. Heath, D. Gatteschi, L. Pardi, R. Sessoli, G. Spina, F. Del Giallo, and F. Pieralli, “Synthesis, structures, and magnetic properties of Fe₂, Fe₁₇, and Fe₁₉ oxo-bridged iron clusters: The stabilization of high ground state spins by cluster aggregates,” *Journal of the American Chemical Society* **117**, 2491–2502 (1995), <https://doi.org/10.1021/ja00114a012>.
- ³⁷C. Cadiou, M. Murrie, C. Paulsen, V. Villar, W. Wernsdorfer, and R. E. P. Winpenny, “Studies of a nickel-based single molecule magnet: resonant quantum tunnelling in an $s = 12$ molecule,” *Chem. Commun.* , 2666–2667 (2001).
- ³⁸M. Murrie, S. J. Teat, H. Stöckli-Evans, and H. U. Güdel, “Synthesis and characterization of a cobalt(II) single-molecule magnet,” *Angewandte Chemie International Edition* **42**, 4653–4656 (2003), <https://onlinelibrary.wiley.com/doi/pdf/10.1002/anie.200351753>.
- ³⁹Y.-Z. Zhang, W. Wernsdorfer, F. Pan, Z.-M. Wang, and S. Gao, “An azido-bridged disc-like heptanuclear cobalt(II) cluster: towards a single-molecule magnet,” *Chem. Commun.* , 3302–3304 (2006).
- ⁴⁰A.-L. Barra, P. Debrunner, D. Gatteschi, C. E. Schulz, and R. Sessoli, “Superparamagnetic-

- like behavior in an octanuclear iron cluster,” *Europhysics Letters (EPL)* **35**, 133–138 (1996).
- ⁴¹O. Waldmann, “A criterion for the anisotropy barrier in single-molecule magnets,” *Inorganic Chemistry* **46**, 10035–10037 (2007), pMID: 17979271, <https://doi.org/10.1021/ic701365t>.
- ⁴²F. Neese and D. A. Pantazis, “What is not required to make a single molecule magnet,” *Faraday Discuss.* **148**, 229–238 (2011).
- ⁴³H. Oshio and M. Nakano, “High-spin molecules with magnetic anisotropy toward single-molecule magnets,” *Chemistry – A European Journal* **11**, 5178–5185 (2005), <https://chemistry-europe.onlinelibrary.wiley.com/doi/pdf/10.1002/chem.200401100>.
- ⁴⁴E. Ruiz, J. Cirera, J. Cano, S. Alvarez, C. Loose, and J. Kortus, “Can large magnetic anisotropy and high spin really coexist?” *Chem. Commun.* , 52–54 (2008).
- ⁴⁵L. M. C. Beltran and J. R. Long, “Directed assembly of metal-cyanide cluster magnets,” *Accounts of Chemical Research* **38**, 325–334 (2005), pMID: 15835879, <https://doi.org/10.1021/ar040158e>.
- ⁴⁶X.-Y. Wang, C. Avendaño, and K. R. Dunbar, “Molecular magnetic materials based on 4d and 5d transition metals,” *Chem. Soc. Rev.* **40**, 3213–3238 (2011).
- ⁴⁷K. S. Pedersen, J. Bendix, and R. Clérac, “Single-molecule magnet engineering: building-block approaches,” *Chem. Commun.* **50**, 4396–4415 (2014).
- ⁴⁸D. N. Woodruff, R. E. P. Winpenny, and R. A. Layfield, “Lanthanide single-molecule magnets,” *Chemical Reviews* **113**, 5110–5148 (2013), pMID: 23550940, <https://doi.org/10.1021/cr400018q>.
- ⁴⁹F.-S. Guo, A. K. Bar, and R. A. Layfield, “Main group chemistry at the interface with molecular magnetism,” *Chemical Reviews* **119**, 8479–8505 (2019), pMID: 31059235, <https://doi.org/10.1021/acs.chemrev.9b00103>.
- ⁵⁰R. Sessoli and A. K. Powell, “Strategies towards single molecule magnets based on lanthanide ions,” *Coordination Chemistry Reviews* **253**, 2328 – 2341 (2009), deutsche Forschungsgemeinschaft Molecular Magnetism Research Report.
- ⁵¹S. G. McAdams, A.-M. Ariciu, A. K. Kostopoulos, J. P. Walsh, and F. Tuna, “Molecular single-ion magnets based on lanthanides and actinides: Design considerations and new advances in the context of quantum technologies,” *Coordination Chemistry Reviews* **346**, 216 – 239 (2017), sI: 42 iccc, Brest– by invitation.

- ⁵²Z. Zhu, M. Guo, X.-L. Li, and J. Tang, “Molecular magnetism of lanthanide: Advances and perspectives,” *Coordination Chemistry Reviews* **378**, 350 – 364 (2019), special issue on the 8th Chinese Coordination Chemistry Conference.
- ⁵³A. Dey, J. Acharya, and V. Chandrasekhar, “Heterometallic 3d–4f complexes as single-molecule magnets,” *Chemistry – An Asian Journal* **14**, 4433–4453 (2019).
- ⁵⁴S. Demir, I.-R. Jeon, J. R. Long, and T. D. Harris, “Radical ligand-containing single-molecule magnets,” *COORDINATION CHEMISTRY REVIEWS* **289**, 149–176 (2015).
- ⁵⁵R. A. Layfield, “Organometallic single-molecule magnets,” *Organometallics* **33**, 1084–1099 (2014).
- ⁵⁶P. Hohenberg and W. Kohn, “Inhomogeneous electron gas,” *Physical Review* **136**, B864–B871 (1964).
- ⁵⁷W. Kohn and L. J. Sham, “Self-consistent equations including exchange and correlation effects,” *Phys. Rev.* **140**, A1133–A1138 (1965).
- ⁵⁸E. Engel and R. M. Dreizler, *Density functional theory* (Springer, 2013).
- ⁵⁹J. C. Slater, “Wave functions in a periodic potential,” *Phys. Rev.* **51**, 846–851 (1937).
- ⁶⁰J. Slater, “Energy band calculations by the augmented plane wave method,” (Academic Press, 1964) pp. 35–58.
- ⁶¹O. K. Andersen, “Linear methods in band theory,” *Phys. Rev. B* **12**, 3060–3083 (1975).
- ⁶²D. D. Koelling and G. O. Arbman, “Use of energy derivative of the radial solution in an augmented plane wave method: application to copper,” *Journal of Physics F: Metal Physics* **5**, 2041–2054 (1975).
- ⁶³L. Zhang, A. Kozhevnikov, T. Schulthess, H.-P. Cheng, and S. B. Trickey, “Performance enhancement of apw+lo calculations by simplest separation of concerns,” *Computation* **10** (2022), 10.3390/computation10030043.
- ⁶⁴“Cuda toolkit documentation,” <https://docs.nvidia.com/cuda/index.html> (), version: v11.2.1.
- ⁶⁵N. M. Josuttis, *The C++ Standard Library: A Tutorial and Reference*, 3rd ed. (Addison-Wesley, Philadelphia, PA, 2000).
- ⁶⁶“Nvcc compiler,” <https://docs.nvidia.com/cuda/cuda-compiler-driver-nvcc/> ().
- ⁶⁷E. Angerson, Z. Bai, J. Dongarra, A. Greenbaum, A. McKenney, J. Du Croz, S. Hammarling, J. Demmel, C. Bischof, and D. Sorensen, “Lapack: A portable linear algebra library for high-performance computers,” in *Supercomputing '90: Proceedings of the 1990*

- ACM/IEEE Conference on Supercomputing* (1990) pp. 2–11.
- ⁶⁸A. Gulans, “Implementation of davidson iterative eigen solver for lapw,” to be published (2015).
- ⁶⁹P. G. Sim and E. Sinn, “First manganese(iii) spin crossover, first d4 crossover. comment on cytochrome oxidase,” *Journal of the American Chemical Society* **103**, 241–243 (1981), <https://doi.org/10.1021/ja00391a067>.
- ⁷⁰Y. Otsuki, S. Kimura, S. Awaji, and M. Nakano, “Magnetocapacitance effect and magnetostriction by the field-induced spin-crossover in [mniii(taa)],” *AIP Advances* **9**, 085219 (2019), <https://doi.org/10.1063/1.5097891>.
- ⁷¹J.-X. Yu, D.-T. Chen, J. Gu, J. Chen, J. Jiang, L. Zhang, Y. Yu, X.-G. Zhang, V. S. Zapf, and H.-P. Cheng, “Three jahn-teller states of matter in spin-crossover system mn(taa),” *Phys. Rev. Lett.* **124**, 227201 (2020).
- ⁷²J. P. Perdew, K. Burke, and M. Ernzerhof, “Generalized gradient approximation made simple,” *Phys. Rev. Lett.* **77**, 3865–3868 (1996).
- ⁷³G. Kresse and J. Furthmüller, “Efficient iterative schemes for ab initio total-energy calculations using a plane-wave basis set,” *Phys. Rev. B* **54**, 11169–11186 (1996).
- ⁷⁴S. Hill, R. S. Edwards, N. Aliaga-Alcalde, and G. Christou, “Quantum coherence in an exchange-coupled dimer of single-molecule magnets,” *Science* **302**, 1015–1018 (2003), <https://science.sciencemag.org/content/302/5647/1015.full.pdf>.
- ⁷⁵A. Wilson, S. Hill, R. S. Edwards, N. Aliaga-Alcalde, and G. Christou, “Entanglement of exchange-coupled dimers of single-molecule magnets,” *AIP Conference Proceedings* **850**, 1141–1142 (2006), <https://aip.scitation.org/doi/pdf/10.1063/1.2355106>.
- ⁷⁶R. Tiron, W. Wernsdorfer, D. Foguet-Albiol, N. Aliaga-Alcalde, and G. Christou, “Spin quantum tunneling via entangled states in a dimer of exchange-coupled single-molecule magnets,” *Phys. Rev. Lett.* **91**, 227203 (2003).
- ⁷⁷T. N. Nguyen, W. Wernsdorfer, K. A. Abboud, and G. Christou, “A supramolecular aggregate of four exchange-biased single-molecule magnets,” *Journal of the American Chemical Society* **133**, 20688–20691 (2011), pMID: 22136491, <https://doi.org/10.1021/ja2087344>.
- ⁷⁸T. N. Nguyen, M. Shiddiq, T. Ghosh, K. A. Abboud, S. Hill, and G. Christou, “Covalently linked dimer of mn3 single-molecule magnets and retention of its structure and quantum properties in solution,” *Journal of the American Chemical Society* **137**, 7160–7168 (2015), pMID: 26027646, <https://doi.org/10.1021/jacs.5b02677>.

- ⁷⁹V. S. Zapf, D. Zocco, B. R. Hansen, M. Jaime, N. Harrison, C. D. Batista, M. Kenzelmann, C. Niedermayer, A. Lacerda, and A. Paduan-Filho, “Bose-einstein condensation of $s = 1$ nickel spin degrees of freedom in $\text{NiCl}_2-4\text{SC}(\text{NH}_2)_2$,” *Phys. Rev. Lett.* **96**, 077204 (2006).
- ⁸⁰S. A. Zvyagin, J. Wosnitza, C. D. Batista, M. Tsukamoto, N. Kawashima, J. Krzystek, V. S. Zapf, M. Jaime, N. F. Oliveira, and A. Paduan-Filho, “Magnetic excitations in the spin-1 anisotropic heisenberg antiferromagnetic chain system $\text{NiCl}_2-4\text{SC}(\text{NH}_2)_2$,” *Phys. Rev. Lett.* **98**, 047205 (2007).
- ⁸¹V. S. Zapf, P. Sengupta, C. D. Batista, F. Nasreen, F. Wolff-Fabris, and A. Paduan-Filho, “Magnetoelectric effects in an organometallic quantum magnet,” *Phys. Rev. B* **83**, 140405 (2011).
- ⁸²V. S. Zapf, V. F. Correa, P. Sengupta, C. D. Batista, M. Tsukamoto, N. Kawashima, P. Egan, C. Pantea, A. Migliori, J. B. Betts, M. Jaime, and A. Paduan-Filho, “Direct measurement of spin correlations using magnetostriction,” *Phys. Rev. B* **77**, 020404 (2008).
- ⁸³M. Yazback, J.-X. Yu, S. Liu, L. Zhang, N. S. Sullivan, and H.-P. Cheng, “First-principles study of an $s = 1$ quasi one-dimensional quantum molecular magnetic material,” *Phys. Rev. B* **103**, 054434 (2021).
- ⁸⁴R. Yu, L. Yin, N. S. Sullivan, J. Xia, C. Huan, A. Paduan-Filho, N. F. Oliveira, S. H. Jr, A. Steppke, C. F. Miclea, F. Weickert, R. Movshovich, E.-D. Mun, B. L. Scott, V. S. Zapf, and T. Roscilde, “Bose glass and mott glass of quasiparticles in a doped quantum magnet,” *Nature* **489**, 379 (2012).
- ⁸⁵A. I. Johnson, F. Islam, C. M. Canali, and M. R. Pederson, “A multiferroic molecular magnetic qubit,” *The Journal of Chemical Physics* **151**, 174105 (2019), <https://doi.org/10.1063/1.5127956>.
- ⁸⁶M. Gakiya Teruya, X. Jiang, D. Le, O. Ungor, A. J. Durrani, J. J. Koptur Palenchar, J. Jiang, T. Jiang, M. W. Meisel, H.-P. Cheng, X.-G. Zhang, X.-X. Zhang, T. S. Rahman, A. F. Hebard, and M. Shatruk, “Asymmetric design of spin crossover complexes to increase the volatility for surface deposition,” *Journal of the American Chemical Society* **143**, 14563–14572 (2021).
- ⁸⁷D. Le, T. Jiang, M. Gakiya-Teruya, M. Shatruk, and T. S. Rahman, “On stabilizing spin crossover molecule $[\text{Fe}(\text{tBu}_2\text{qsal})_2]$ on suitable supports: insights from ab initio studies,” *Journal of Physics: Condensed Matter* **33**, 385201 (2021).
- ⁸⁸D. Vanderbilt, “Soft self-consistent pseudopotentials in a generalized eigenvalue formal-

ism,” Phys. Rev. B **41**, 7892–7895 (1990).

⁸⁹G. Kresse and D. Joubert, “From ultrasoft pseudopotentials to the projector augmented-wave method,” Phys. Rev. B **59**, 1758–1775 (1999).

⁹⁰C.G.Broyden, “A class of methods for solving nonlinear simultaneous equations,” Math. Comm. **19**, 577–593 (1965).

⁹¹H.-r. Fang and Y. Saad, “Two classes of multiseant methods for nonlinear acceleration,” Numerical Linear Algebra with Applications **16**, 197–221 (2009), <https://onlinelibrary.wiley.com/doi/pdf/10.1002/nla.617>.